

# Calibration of VELC detectors on-board Aditya-L1 mission

Shalabh Mishra<sup>1</sup>, K. Sasikumar Raja<sup>1\*</sup>, Sanal Krishnan V  
U<sup>1</sup>, Venkata Suresh Narra<sup>1</sup>, Bhavana Hegde S<sup>1</sup>, Utkarsha  
D.<sup>1</sup>, Muthu Priyal V<sup>1</sup>, Pawan Kumar S<sup>1</sup>, Natarajan  
V<sup>1</sup>, Raghavendra Prasad B<sup>1</sup>, Jagdev Singh<sup>1</sup>, Umesh Kamath  
P<sup>1</sup>, Kathiravan S<sup>1</sup>, Vishnu T<sup>1</sup>, Suresha<sup>1</sup>, Savarimuthu  
P<sup>1</sup>, Jalshri H Desai<sup>2</sup>, Rajiv Kumaran<sup>2</sup>, Shiv Sagar<sup>3</sup>, Sumit  
Kumar<sup>2</sup>, Inderjeet Singh Bamrah<sup>2</sup> and Amit Kumar<sup>1</sup>

<sup>1\*</sup>Indian Institute of Astrophysics, 2nd Block, Koramangala,  
Bangalore, 560034, Karnataka, India.

<sup>2</sup>Space Applications Centre, ISRO, Satellite Road, Ahmedabad,  
380015, Gujarat, India.

<sup>3</sup>U R Rao Satellite Centre, ISRO, HAL Old Airport Road,  
Bengaluru, 560017, Karnataka, India.

\*Corresponding author(s). E-mail(s): [sasikumar.raja@iiap.res.in](mailto:sasikumar.raja@iiap.res.in);

## Abstract

Aditya-L1 is the first Indian space mission to explore the Sun and solar atmosphere with seven multi-wavelength payloads, with Visible Emission Line Coronagraph (VELC) being the prime payload. It is an internally occulted coronagraph with four channels to image the Sun at 5000 Å in the field of view 1.05 - 3  $R_{\odot}$ , and to pursue spectroscopy at 5303 Å, 7892 Å and 10747 Å channels in the FOV (1.05 - 1.5  $R_{\odot}$ ). In addition, spectropolarimetry is planned at 10747 Å channel. Therefore, VELC has three sCMOS detectors and one InGaAs detector. In this article, we aim to describe the technical details and specifications of the detectors achieved by way of thermo-vacuum calibration at the CREST campus of the Indian Institute of Astrophysics, Bangalore, India. Furthermore, we report the estimated conversion gain, full-well capacity, and readout noise at different temperatures. Based on the numbers, it is thus concluded that it is essential to operate the sCMOS detectors and InGaAs detectors at  $-5^{\circ}$  and  $-17^{\circ}$  C, respectively, at the spacecraft level.

**Keywords:** Aditya-L1, VELC, sCMOS detectors, InGaAs detectors

## 1 Introduction

ADITYA-L1 is the first Indian solar space mission that is expected to provide valuable insights on solar dynamics with seven payloads on board [1]. Visible Emission Line Coronagraph (VELC), an internally occulted coronagraph, is the prime payload of the mission with imaging, spectroscopy, and spectropolarimetry channels being concomitantly operational for observation close to the solar limb [2, 3]. The configuration of VELC is to enable the payload in order to image solar corona at  $5000\text{\AA}$  from  $1.05 R_{\odot}$  to  $3 R_{\odot}$  ( $R_{\odot}$  represents the solar radii) (i.e.,  $0.28^{\circ}$  -  $0.8^{\circ}$ ) with a plate scale of  $2.5''/\text{pixel}$  [2].

The design configuration of VELC facilitates synchronous spectroscopic observations at three solar emission lines i.e., Fe XIV (at  $5303\text{\AA}$ ), Fe XI (at  $7892\text{\AA}$ ) and Fe XIII (at  $10747\text{\AA}$ ) with a distinct spectral resolution of 28, 31 and  $202 \text{ m\AA}/\text{pixel}$  respectively, over the field of view (FOV) of  $1.05 R_{\odot}$  to  $1.5 R_{\odot}$  (i.e.,  $0.28^{\circ}$  to  $0.4^{\circ}$ ) [2]. The Fe XIII (at  $10747\text{\AA}$ ) channel also facilitates to study coronal magnetic fields using dual-beam spectropolarimetry.

The observations in the solar imaging channel at  $5000\text{\AA}$  alongside spectroscopic observations at  $5303\text{\AA}$  and  $7892\text{\AA}$  are accomplished using an sCMOS detector with good spectral response in a range of  $4000\text{-}7000\text{\AA}$ . The spectroscopy and spectro-polarimetry observations at  $10747\text{\AA}$  are accomplished using an InGaAs detector with spectral response in the range of  $9000\text{-}17000\text{\AA}$ . The complex thermal management of the payload ensures that the stringent requirement of chip temperatures at each detector is achieved. The functional control of parameters such as bias, temperature, etc., are augmented to achieve the best in-orbit performance of the payload.

The detector electronics comprises primarily three functional modules, namely, the Detector Proximity Electronics (DPE), Digital Control and Processing Electronics (DCPE), and Payload Power Electronics (PPE). The DPE comprises the detector, its bias, and the data and clock interface. DCPE receives the clock and transmits the serialized data. It is also responsible for generating control signals and data processing, including onboard intelligence for CME detection [4]. PPE addresses the power requirements of the modules above. The detector electronics interfaces with Onboard computer (OBC) and Onboard Data Handling and Storage (ODHS) unit for payload functionality including commanding and data acquisition and onboard data storage.

## 2 Technical details of the detectors

The Detector Head Assembly (DHA) incorporates the area array imaging sensor, mechanical interface of DHA for precision mounting on the optical bench of VELC, cold finger thermal interface for optimal temperature control and

DPE. The perspicacity to perceive the science objectives of the payload and accordingly determine the optimal imaging sensor to carry out the operations.

## 2.1 Scientific grade CMOS sensor

High-speed imaging, high resolution, and exceptionally low readout noise enable the utilization of scientific grade CMOS CIS2051 sensor for VELC payload in imaging and two spectroscopy channels, i.e. 5303Å and 7892Å. The sensor comprises an array of 2160(H)×2560(V) photodiodes with a pixel dimension of 6.5μm×6.5μm. The sensor is divided into two independent sections (1080×2560 top and bottom card) with independent controls. The sensor is equipped with dual column-level amplifiers so that it can be configured for either 1X or 2X analog gains in Low Gain mode and 10X or 30X analog gains in High Gain mode. The output of both the amplifier levels is concurrently provided to dual-level 11-bit ADCs. Considering the design framework, at any juncture, 22-bit pixel data corresponding to both the gains (11-bit each) for each half of the sensor is available for readout.

The vital specifications of the sCMOS detector electronics are detailed in Table 1.

**Table 1:** Specifications of sCMOS detector

S. No.	Parameter	Description
1.	Sensor Format	2160 × 2560
2.	Pixel Size	6.5μm × 6.5μm
3.	Spectral Range	4000 Å to 9000 Å
4.	Readout Mode	Rolling Shutter
5.	Number of ports	Two (22-bit) (11-bit low gain, 11-bit high gain)
6.	Gain	Four (1X, 2X, 10X, 30X)
7.	Integration time	10ms to 100sec
8.	Detector configuration mode	JTAG
9.	Operating Mode	Read then integration
10.	Pixel Readout (MHz)	52.5
11.	Data Rate (Mbps)	52.5 parallel
12.	Payload data interface	SerDes

## 2.2 InGaAs FPA sensor

Accommodating the sensor non-uniformity, dark current, full-well capacity, and longer integration times, the InGaAs 640×512 focal plane photodiode array from Chungwa is utilized in the DHA fabrication for the spectropolarimetry channel of VELC. The sensor is responsive in the SWIR band, i.e., 9000Åto 17000Å. The sensor is fabricated such that the photodiode array is attached to the Readout Integrated Circuit (ROIC) utilizing indium bumps.

Considering the notable integration times, appreciable in comparison to the readout time of the detector, integrate while read (IWR) methodology of operation is preferred. The detector output is read out using a single port, which provides an analog output. The output is digitized (12-bit) in FECE (Front-End Camera Electronics) and provided to DCPE through 3V CMOS interface for further processing. The vital specifications of the IR detector electronics are detailed in Table 2.

**Table 2:** Specifications of IR detector

S. No.	Parameter	Description
1.	Sensor Format	512 × 640
2.	Pixel Size	25 $\mu$ m × 25 $\mu$ m
3.	Spectral Range	9000 Å to 17000 Å
4.	Readout Mode	Rolling Shutter
5.	Number of ports	One
6.	Gain	Two (LG, HG)
7.	Integration time	50ms to 100sec
8.	Detector configuration mode	Serial
9.	Operating Mode	Read while integration
10.	Pixel Readout (MHz)	6.56
11.	Data Rate (Mbps)	26.25 serial
12.	Payload data interface	3V LVDS

### 3 Thermo vacuum-chamber and calibration setup

VELC has a complex thermal management system considering all the different subsystems and a stable operational temperature at the sensor chip is paramount. During the stand-alone testing of the detectors, the desired temperature was obtained by connecting one end of the mini-heat pipe to detector head assembly and the other end to the external Thermal Control Unit (TCU) via heat exchanger for the thermal flow as shown in Figure-1. Note that after integration of the payload, TCU was replaced by a radiator plate. The details on the coupling of the detectors and the radiator plate will be presented elsewhere.

Considering the limitation in mounting a temperature sensor at the detector chip, the closest place for monitoring is at the cooling plate interface. Therefore, a calibration setup, as shown in Figure 1, is designed to estimate the temperature gradient between the detector chip and cooling plate interface by simulating the inherent detector power dissipation using a heater. A sensor is placed at the detector chip interface and another at the cooling plate interface. The test was carried out to measure all the desired chip temperature levels for both sCMOS (visible) and InGaAs (IR) detectors.

Considering the science objectives of the payload along with the system limitations in terms of scatter and efficiency, the dark response of the DHAs, along with performance at various integration times and temperature, becomes of paramount importance [5]. The DHA calibration inside the thermo-vacuum chamber (TVAC), as shown in Figure 1, was carried out at various temperature levels in order to determine the absolute operating temperature for the respective DHAs to corroborate optimum system performance. The calibration was carried out at  $10^{-5}$  mbar vacuum with a thermal control unit established to provide a temperature stability of  $0.5^\circ$  C.

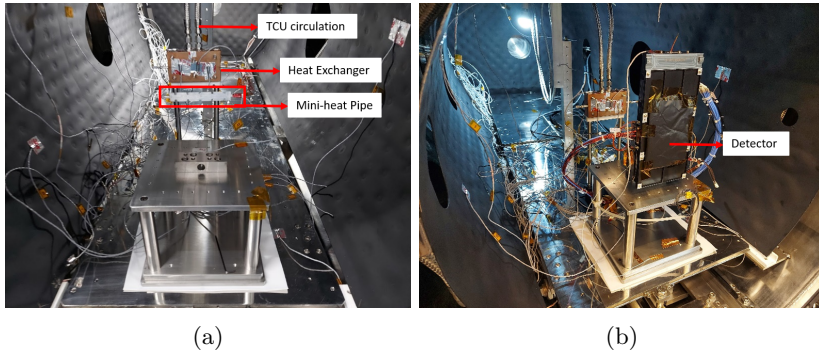


**Fig. 1:** Subplot (a) shows the cooling plate interface calibration unit and Subplot (b) shows the DHA after mounting in Thermo Vacuum Chamber for calibration at CREST campus of the Indian Institute of Astrophysics.

## 4 Results and Discussions

Set of dark frames of integration time that range from 10ms to 100s is obtained for visible detectors and 50ms to 100s is obtained for IR detector. Furthermore, for flat-fielding, light exposures are acquired with different exposure times such that  $\approx 80 - 90\%$  of the full well capacity is attained. Since the readout for visible and IR detectors is 11-bit and 12-bit respectively, the integration time varies based on the specified gain (during light exposures) and by illuminating the constant flux on the detectors. The dark images obtained using visible and IR detectors is as shown in Figure 2 and Figure 3, respectively.

### 4.1 Estimation of mean and standard deviation of the images

If 'i' and 'j' represent the pixel coordinates and 'z' represents the frame number, the image  $I_z(i, j)$  represents the intensity values of  $z^{th}$  frame at  $(i, j)^{th}$  pixel coordinates. To measure the mean dark counts and standard deviation of the images, if the integration time is greater than 20s, we acquired eight frames,

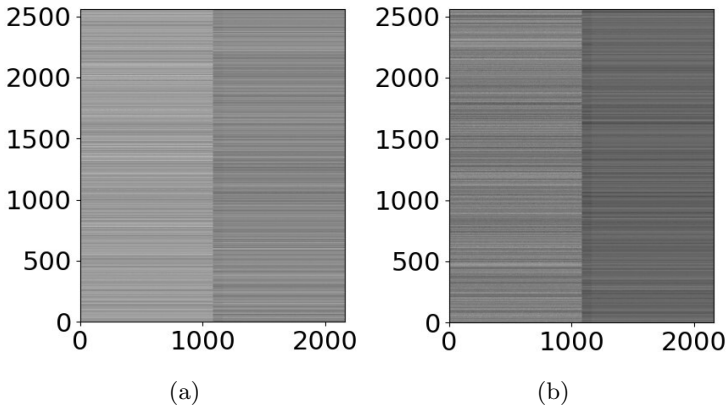


**Fig. 2:** Subplot (a) shows the combined low gain image of both top and bottom card of sCOMS detector and subplot (b) shows the combined high gain image of both top and bottom card of the sCMOS detector

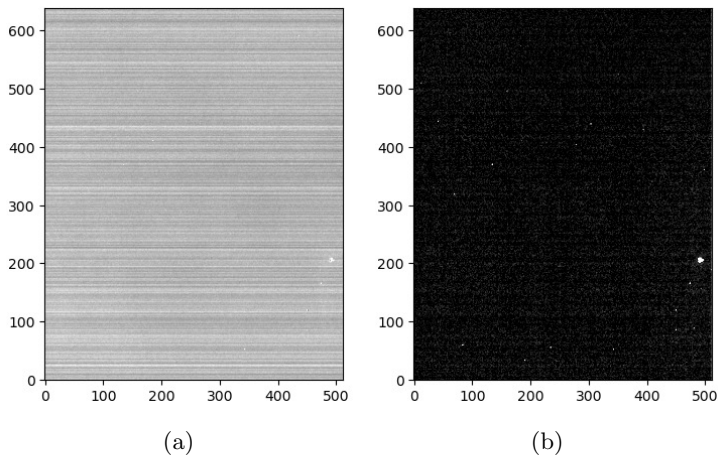


**Fig. 3:** Subplots (a) and (b) shows the low gain and high gain images of InGaAs detector respectively

and if the integration time is less than or equal to 20s, we acquired 16 frames per set.

### 4.1.1 Mean calculation

First, pixel-to-pixel mean of all frames is calculated over the entire frame acquired using the relation

$$I(i, j) = \frac{1}{n} \sum_{z=1}^n I_z(i, j) \quad (1)$$

where  $n$  is the number of frames acquired and  $I(i, j)$  is the image of each pixel averaged over all the frames. Then mean of  $I(i, j)$  is calculated using,

$$Mean = \frac{1}{N \times M} \sum_{i=1}^N \sum_{j=1}^M I(i, j) \quad (2)$$

where  $N$  and  $M$  represents the pixel coordinates.

### 4.1.2 Standard deviation calculation

First, pixel-to-pixel standard deviation of all frames is calculated over the entire frame acquired using the relation

$$\sigma(i, j) = \sqrt{\frac{1}{n-1} \sum_{z=1}^n (I_z(i, j) - \overline{I(i, j)})^2}, \quad (3)$$

where  $\sigma(i, j)$  represents the standard deviation matrix and  $\overline{I(i, j)}$  represents the mean of the  $I(i, j)$  as discussed in Section 4.1.1.

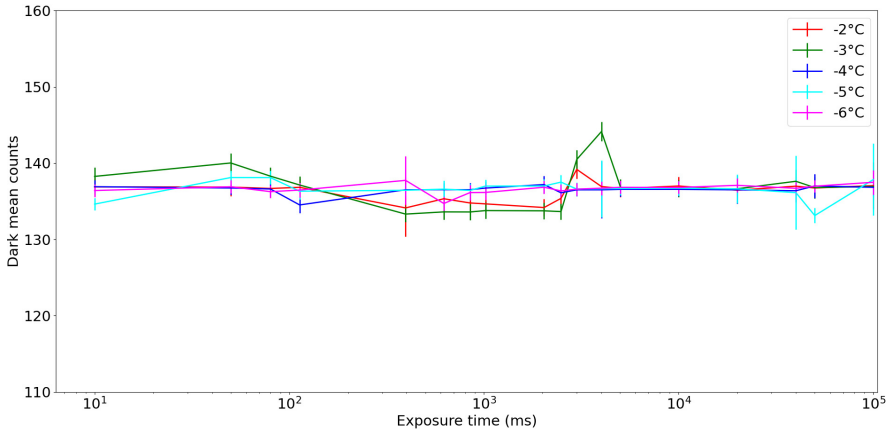
Furthermore, the standard deviation is obtained by averaging the acquired  $\sigma(i, j)$  matrix using,

$$SD = \frac{1}{N \times M} \sum_{i=1}^N \sum_{j=1}^M \sigma(i, j) \quad (4)$$

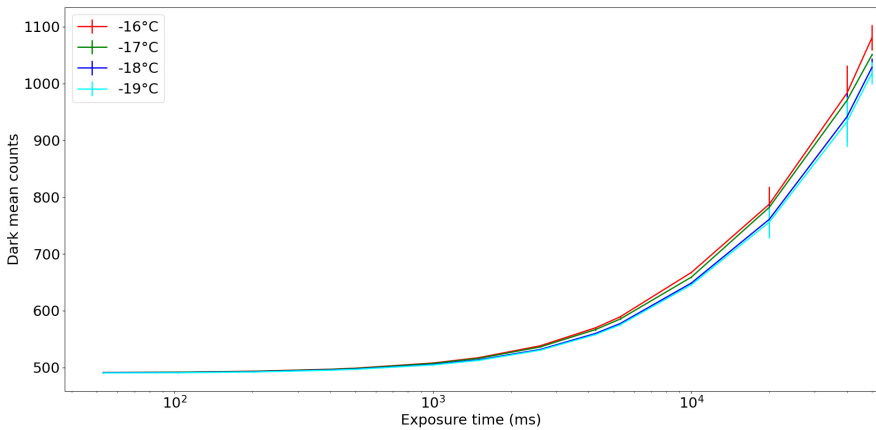
The measured mean and standard deviation with respect to exposure time of acquired dark and light images for both visible and IR detectors at various temperatures is as shown in Figure 4 and Figure 5.

## 4.2 Estimation of detector parameters

Using the light and dark data we estimated conversion gain, full-well capacity and read noise values using the standard method described in the following subsections [for example refer 6–9].



(a) Mean dark variation for sCMOS with deviation as error bar

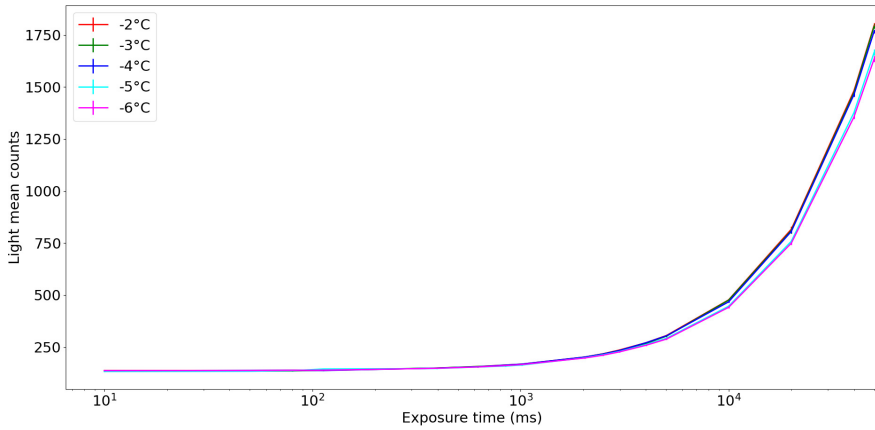


(b) Mean dark variation for IR with deviation as error bar

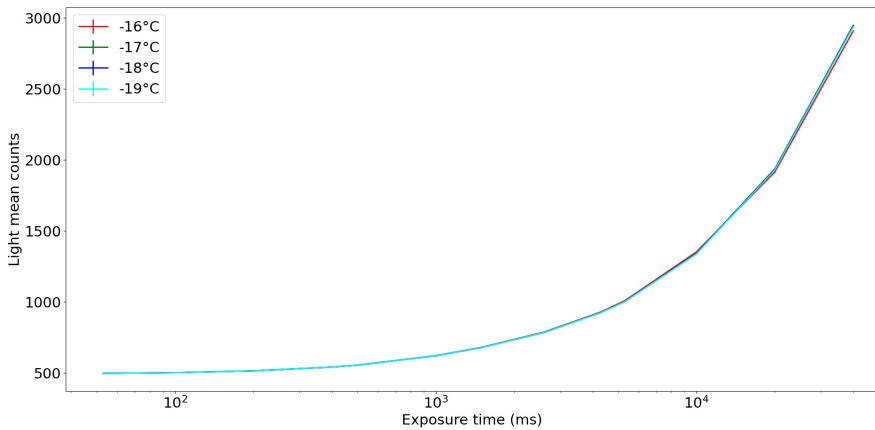
**Fig. 4:** Mean dark variation for sCMOS and IR detectors

### 4.2.1 Conversion Gain

The conversion gain is measured from the photon transfer curve obtained from the curve of variance with the mean photon counts during the light exposures of the detector. The curve is then fitted with line equation  $y = mx + c$  where 'm' and 'c' are the slope and intercept of the curve. Furthermore, the conversion gain is calculated by taking the inverse of the obtained slope. The conversion gain of the visible detector is tabulated in Table 3, and the IR detector is tabulated in Table 4.



(a) Light exposures for sCMOS with deviation as error bar



(b) Light exposures for IR with deviation as error bar

**Fig. 5:** Light exposures for sCMOS and IR detectors**Table 3:** Conversion Gain in  $e^-/DN$  of visible detector

S. No.	Gain	$T = -2^\circ C$	$T = -3^\circ C$	$T = -4^\circ C$	$T = -5^\circ C$	$T = -6^\circ C$
1.	1X	14.85	14.70	15.87	15.55	15.29
2.	2X	8.92	8.77	9.07	8.48	8.82
3.	10X	2.12	2.08	1.88	1.69	1.69
4.	30X	0.61	0.57	0.56	0.52	0.54

**Table 4:** Conversion Gain in  $e^-/DN$  of IR detector

S. No.	Gain	$T = -16^\circ C$	$T = -17^\circ C$	$T = -18^\circ C$	$T = -19^\circ C$
1.	LG	768.13	790.65	779.62	781.84
2.	HG	11.22	12.07	10.59	11.49

### 4.2.2 Full Well Capacity

The full-well capacity is obtained by multiplying the conversion gain with the mean counts when nearly 90% of the saturation counts are achieved with light exposures. The full-well capacity of the visible detector is tabulated in Table 5, and for IR detector is tabulated in Table 6.

**Table 5:** Full well capacity in  $ke^-$  of visible detector

S. No.	Gain	$T = -2^\circ C$	$T = -3^\circ C$	$T = -4^\circ C$	$T = -5^\circ C$	$T = -6^\circ C$
1.	1X	24.64	24.12	25.87	23.97	23.10
2.	2X	12.97	12.14	12.96	11.29	11.49
3.	10X	3.52	3.43	3.09	2.57	2.52
4.	30X	1.01	0.9	0.9	0.98	0.99

**Table 6:** Full Well Capacity in  $ke^-$  of IR detector

S. No.	Gain	$T = -16^\circ C$	$T = -17^\circ C$	$T = -18^\circ C$	$T = -19^\circ C$
1.	LG	1857.73	1943.72	1912.28	1913.82
2.	HG	25.37	27.44	23.42	24.98

### 4.2.3 Read Noise

Read noise is obtained by multiplying the conversion gain with the standard deviation value for minimum possible exposure in the dark. The read noise of the visible detector is tabulated in Table 7, and the IR detector is tabulated in Table 8.

The Thermovac (TVAC) test of complete payload was carried out as part of environmental tests with complete thermal control in place. The dark counts of the detectors obtained during the standalone tests show a good correlation with the darks obtained during payload level (integrated VELC alone) and spacecraft level (after integration of the VELC and other payloads with the spacecraft). Light exposures were taken only during the subsystem level tests and repetition of the same was not possible during the TVAC tests due

**Table 7:** Read noise in  $e^-$  of visible detector

S. No.	Gain	$T = -2^\circ C$	$T = -3^\circ C$	$T = -4^\circ C$	$T = -5^\circ C$	$T = -6^\circ C$
1.	1X	17.08	16.91	13.81	12.75	12.69
2.	2X	9.64	7.98	7.98	7.71	7.14
3.	10X	10.02	9.60	9.49	8.42	8.52
4.	30X	3.62	3.53	3.58	3.50	3.53

**Table 8:** Read noise in  $e^-$  of IR detector

S. No.	Gain	$T = -16^\circ C$	$T = -17^\circ C$	$T = -18^\circ C$	$T = -19^\circ C$
1.	LG	988.33	956.15	942.31	865.0
2.	HG	18.25	15.89	14.54	13.69

to the contamination protocols. However, experiments related to payload calibration with solar disk light were carried out and the same was reported by Raghavendra Prasad et al [10].

VELC entrance aperture has a 45 mm neutral density filter with density 4 and that allows the part of the Sun light when pointed towards the Sun. Therefore, it planned to point the spacecraft by 15-30 degrees away from the centre of the Sun and keep the EA door in closed condition and acquire the dark data. Similar dark measurements are planned to be carried out once in a three months for the entire mission lifetime. Such measurements help understand whether the onboard dark measurements are matching with the ones obtained during the ground based calibration and how the dark counts are varying with the mission life [11].

Further it is planned to carry out the disk images and disk spectral observations by pointing the spacecraft by 16 and 32 arcmin away from the disk centre and keeping the EA door in closed condition. When we off-point the spacecraft by 32 arcmin in four directions (say east, west, south and north) the disk of the Sun will appear in the field of view (FOV). When we off-point the spacecraft by 16 arcmin in four directions (say east, west, south and north), the centre of the Sun will fall in the slits and disk spectra can be obtained. Such observations will help understand the pixel response of the detector for the light [11].

## 5 Summary and Conclusions

In this article, we discussed various technical details and specifications of the sCMOS and InGaAs detectors used in the Visible Emission Line Coronagraph. Furthermore, we presented the ground calibration methodology that opted to calibrate the detectors in the thermo-vacuum chamber located at the CREST campus of IIA. Using the observed parameters, we have estimated conversion

gains, full-well capacity, readout noise, etc, for the detectors at various temperatures. Using such parameters, we concluded that operating the sCMOS and InGaAs detectors at  $-5^{\circ}$  and  $-17^{\circ}$  C onboard is essential.

**Acknowledgments.** We thank all the Scientists/Engineers at the various centres of ISRO such as URSC, SAC, LEOS, VSSC etc. and Indian Institute of Astrophysics who have made great contributions to the mission in order to achieve the present state. We thank anonymous referee for providing valuable suggestions that improved the manuscript.

**Author's contributions:** SM and KSR analysed the data and wrote the manuscript. SM, KSR, SKVU, BH, UD involved in calibration activities and acquiring the data. BRP, JS, VSN, AK provided the inputs with the setup, designing calibration procedures etc and also reviewed the manuscript. MP and SP helped with the data analysis. PUK, PK, NV, KS, VT, Suresha extended their help with the ETF facility, mounting the detectors in the TVAC chamber, maintaining the pressure and temperatures at desired levels etc. JHD, RK, SS, SK, ISB are the designers of the hardware electronics related to the detectors.

**Funding** We gratefully acknowledge the financial support from Indian Space Research Organization (ISRO), India for this project.

## Declarations

**Competing interests:** The authors declare no competing interests.

**Conflicts of interest:** The authors declare that they have no conflict of interest.

## References

- [1] S. Seetha and S. Megala. Aditya-L1 mission. *Current Science*, 113(4):610, August 2017.
- [2] Budihal Prasad, Dipankar Banerjee, Jagdev Singh, Nagabhushana Subramanya, Amit Kumar, P. Kamath, s Kathiravan, Suresh Venkata, N. Rajkumar, Natarajan Venkatasubramanian, Madhur Juneja, Pawan Somu, Vaibhav Pant, K. Sankarsubramanian, Asit Patra, R. Venkateswaran, Abhijit Adoni, S. Narendra, and Bhavesh Jaiswal. Visible emission line coronagraph on aditya-l1. *Current Science*, 113:613–615, 08 2017.
- [3] Jagdev Singh, B. Raghavendra Prasad, Suresh Venkata, and Amit Kumar. Exploring the outer emission corona spectroscopically by using Visible Emission Line Coronagraph (VELC) on board ADITYA-L1 mission.

*Advances in Space Research*, 64(7):1455–1464, October 2019.

- [4] Ritesh Patel, K. Amareswari, Vaibhav Pant, Dipankar Banerjee, K. Sankarasubramanian, and Amit Kumar. Onboard Automated CME Detection Algorithm for the Visible Emission Line Coronagraph on ADITYA-L1. *Solar Physics*, 293(7):103, July 2018.
- [5] J. Postma, J. B. Hutchings, and D. Leahy. Calibration and Performance of the Photon-counting Detectors for the Ultraviolet Imaging Telescope (UVIT) of the Astrosat Observatory. *Publications of the Astronomical Society of the Pacific*, 123(905):833, July 2011.
- [6] James R. Janesick. *Photon Transfer DN  $\rightarrow$   $\lambda$* . 2007.
- [7] S. Karpov, A. Christov, A. Bajat, R. Cunniffe, and M. Prouza. Characterization of Modern CCD and CMOS Sensors for Sky Surveys. In *Revista Mexicana de Astronomia y Astrofisica Conference Series*, volume 53 of *Revista Mexicana de Astronomia y Astrofisica Conference Series*, pages 190–197, September 2021.
- [8] Peng Qiu, Yong Zhao, Jie Zheng, Jian-Feng Wang, and Xiao-Jun Jiang. Research on performances of back-illuminated scientific CMOS for astronomical observations. *Research in Astronomy and Astrophysics*, 21(10):268, November 2021.
- [9] Sanjay Gosain, Jack Harvey, Detrick Branson, Steve Bounds, Tim Purdy, Sang Nguyen, and Greg Card. GONG third generation camera: Detector selection and feasibility study. *arXiv e-prints*, page arXiv:2212.03963, December 2022.
- [10] Raghavendra Prasad Budihal, Venkata Suresh Narra, Natarajan Venkata-subramanian, Pawan Kumar Somasundaram, Umesh Kamath Padavu, Shalabh Mishra, Bhavana Hegde, Sasikumar Raja Kantepalli, and Jagdev Singh. Ground calibration of visible emission line coronagraph on board Aditya-L1 mission. *Journal of Astronomical Telescopes, Instruments, and Systems*, 9(4):044001, 2023.
- [11] Jagdev Singh, B. Raghavendra Prasad, Chavali Sumana, Amit Kumar, Varun Kumar, Muthu Priyal, and Suresh Venkata. Data pipeline architecture and development for VELC onboard Space Solar Mission AdityaL1. *Advances in Space Research*, 69(6):2601–2610, March 2022.